Implementation of Virtual Synchronous Machine Control Using EV Battery's SOC for Single-Stage Converter During Battery Charging

Kabir Momoh*, Shamsul Aizam Zulkifli *‡, Petr Korba **‡, Felix Rafael Segundo Sevilla **, Alfredo Velazquez-Ibañez **, Arif Nur Afandi ***

*Department of Electrical Engineering, Faculty of Electrical and Electronic Engineering (FKEE), Universiti Tun Hussein Onn Malaysia, Batu Pahat 86400, Johor, Malaysia.

** School of Engineering, Zurich University of Applied Sciences, Technikumstrasse 9, 8401 Winterthur, Switzerland.

***Faculty of Engineering, Universitas Negeri Malang, Jl. Semarang 5, Malang, 65145, Malang, Indonesia.

(he200018@student.uthm.edu.my, aizam@uthm.edu.my, korb@zhaw.ch, segu@zhaw.ch, vela@zhaw.ch, an.afandi@um.ac.id)

‡Corresponding Authors; Shamsul Aizam Zulkifli, Faculty of Electrical and Electronic, Engineering (FKEE), Universiti Tun Hussein Onn Malaysia, Batu Pahat 86400, Johor, Malaysia, Tel: +60123487636, aizam@uthm.edu.my, Petr Korba, School of Engineering, Zurich University of Applied Sciences, Technikumstrasse 9, 8401 Winterthur, Switzerland, Tel:+41795423302, korb@zhaw.ch

Received: 07.09.2023 Accepted:29.10.2023

Abstract- The increasing adoption of electric vehicles (EVs) has necessitated the development of advanced controllers during battery charging. Those controllers are vital for maintaining current stability at the point of common coupling (PCC) during battery charging and the power flow response to the battery in order to maintain the battery's voltage. This paper introduces an improved virtual synchronous machine (i-VSM) control using the battery's state-of-charge (SOC) voltage as the virtual flux model for the motor's concept. The i-VSM model adapted the SOC condition, the grid phase angle for power demand, and the reactive power flow between the PCC and the EV. A three-phase rectifier converter behaving as a fast-charging station (FCS) module was integrated into the i-VSM model to reflect the EV battery's SOC condition. The i-VSM model was verified in MATLAB software in order to demonstrate grid stability quality, especially on grid-side current total harmonic distortion (THD) and in maintaining the voltage at the PCC. In the simulation, the i-VSM model was tested with an FCS rated at 150 kW. The virtual inertia maintains the frequency control at PCC and reduces the power oscillation when the load at the PCC was increased from 50 kW to 150 kW. The grid-side current THD was at 3.67%, which was the allowable value at the PCC. If this proposed controller is implemented in future power stations, the FCSs will not affect the grid's condition, and furthermore the controller will increase grid stability and is able to maintain the voltage of different-rated EVs.

Keywords EV battery, state of charge, virtual synchronous motor.

Nomenclature

A, Ah	Ampere, ampere-hour
C, C_{DC}, CC, CV	Filter capacitor, DC link capacitor, charging current, charging voltage
C-rate	Discharge rate

D_q, D_p	Reactive droop regulation loop gain, frequency loop feedback gain
e, e_{abcsoc} , EVs	Electromotive force, electromotive force at SOC consideration, electric vehicles
e_1, e_2, e_3	Three-phase source AC voltage
FCS	Fast charging station
H, Hz	Henry, hertz
i-VSM	Improved virtual synchronous motor
I_B, i_a, i_b, i_c	Battery current, three-phase source AC current
J	Virtual inertia
K_i, Kp, K_q, kW	Integral constant, proportional gain constant, VSM gain constant, Kilowatts
K_v	Voltage regulation constant due to the SOC,
L, L_S	Filter inductor, VSM stator inductance
M_fI_f,M_fI_{fsocrq}	Field excitation, field excitation due to SOC condition
PWM, PI, PF	Pulse-width modulation, Proportional-integral, power factor
Pe, Pm, PCC	Electrical power, mechanical power, point of common coupling
P, PLL, PRef	Active power, phase-lock loop, reference active power
Q, Q_{Ref} ,Q_{rq}	Reactive power and reference reactive power, Reactive power regulation
Q1-Q6	Insulated-gate bipolar transistor (IGBTs)
R_S	VSM stator resistance
SOC	State-of-charge
T_e, T_m, THD	Electrical torque, mechanical torque, total harmonic distortion
VSM, V_{SOCrq}	Virtual synchronous motor Automatic voltage regulation at SOC condition
V_{DCSOC},V_{DCRef}	FCS output voltage at SOC condition, reference FCS rectifier's output voltage
V, V_{abc} , $V_{DCSOCfb}$	Volts, AC voltage of grid, FCS output feedback voltage at SOC condition
V_B, X, Y	Battery voltage, discharging, charging under the SOC condition
μs, μF, Mh ,Ω	Microseconds, microfarad, microhenry, ohms
θ, θ_g , ⟨.,.⟩	Virtual rotor angle, grid angle, Conventional dot product for three phase system
τ_k,ω, ω_{Ref}	Time constant, virtual angular frequency and reference virtual angular frequency

1. Introduction

The growing trend of electric vehicle (EV) penetration and connection to electric power grids have been identified as the major cause of grid instabilities in recent times [1]. This is due to the significant influence of high harmonic current emission by fast-charging stations (FCSs) in power grids [2] during charging operations. FCSs contribute to high-power, nonlinear and discontinuous EV battery load patterns [3] to the grid. These nonlinearities in EV stations create problems, such as voltage dip and frequency and power exchange issues at the point of common coupling (PCC), when multiple EVs are being charged [4] at the same time. At the moment, FCSs consist of two stages of converters, where the first is the rectifier stage and the second is the DC-to-DC converter stage, to transfer power from the electrical grid to the battery for the charging process [5] while maintaining the voltage at the PCC. However, the

report in [6] highlighted high switching losses and complex control circuitry for the two stages of converters, resulting in frequency and power exchange instability [6]. The solution to the two-stage converter is using a single stage to reduce grid current harmonics and power losses from the grid to the battery [7] and also contribute to frequency and voltage control stability during the charging operation.

As for the control mechanism for the converters, several types of proportional-integral (PI) feedback controllers were discussed in [8, 9]. However, these PI-based controllers are prone to complex control stability issues, such as inner-loop, outer-loop and power loop controllers often having a slow dynamic response, unlike the structure using the virtual synchronous machine (VSM) control concept. Therefore, VSM control is an emerging control strategy for simulating the functionality and characteristics of the conventional synchronous machine (SM) for converters, and it can contribute to high-quality voltage or current [10, 11] control at the rectification stage if used for EV battery charging [12, 13]. This controller helps to improve the controller's capability of adjusting the virtual inertia/field winding during the FCS operation, as mentioned in [14, 15]. It works by eliminating the rotating machine's frequency dependence and decoupling the sources from the grid [16, 17], where the angle of the VSM is proportional to the electrical grid's phase angle for faster synchronization for power delivery to the battery. Consequently, the present paper is regarding the adaptability of the virtual synchronous motor when using the EV battery's state-of-charge (SOC) voltage as a new input parameter for the VSM controller to maintain the voltage of the battery. This is because the SOC indicates the EV battery's current level of percentage charge [18, 19]. Without considering the battery's SOC, the controller may not be able to accurately determine the optimal charging rate for maximizing the EV battery's life cycle [20-22,], and it also might not be able to maintain a stable grid voltage nor improve the THD of grid current.

During battery charging, a VSM needs to maintain a stable output voltage at the PCC and provide power flow control to the EV battery [23, 24]. This is to ensure that the charging process remains within safe and optimal operating limits [25]. By actively managing the reactive power flow [26], the VSM can maintain a power factor close to unity [27] for grid voltage and current through the VSM's fast dynamic response in order to minimize the impact on the grid [28]. As stated in [27-30], a VSM can quickly adjust its output to match charging requirements by solving the problem of low inertia issues at the grid through the controllable power balancing approach and power quality improvement. Therefore, research efforts have been redirected to delivering support to the grid via FCS converters enhancement of voltage and active power output adaptability and absorbing the reactive power needed for the inertia support of the grid system.

The contribution of this paper is replacing the PI controller in the VSM control scheme with the proposed improved VSM (i-VSM) model using a single-stage rectifier converter with a SOC voltage feedback controller. At the grid, the proposed controller aimed to maintain a stable output voltage and power flow between the electrical grid and the EV battery regardless of load changes for power factor improvement at the PCC. This paper is structured into the following sections: the proposed i-VSM controller with the droop interface compensation strategy is discussed in Section 2 and the simulation analysis is discussed in Section 3, followed by the conclusion in Section 4.

2. Proposed i-VSM Controller with Droop Interface Compensation Strategy

The proposed controller model was initially outlined as a dynamic system from the perspective of system analysis and controller by setting the number of pole pairs per phase of the VSM as one, similar to the demonstration in [31] as the reference. In the proposed topology, the VSM is integrated with a single-stage rectifier to convert AC power from the grid into DC power to optimize the charging process of the EV battery. This concept incorporates the real time adjustment of the EV battery charge rate at initial SOC condition through the direct feedback of the DC voltage at SOC to the VSM. This topology allows the VSM to maintain regulation of the grid frequency, voltage, power factor and power exchange while ensuring stability of the FCS output DC voltage control during transient similar to SM. The expressions of VSM rotor ($J(d\omega/dt)$), active power-frequency, terminal voltage, virtual inertia (J), mechanical (P_m) and electrical power (P_e) for a VSM controller are derived in terms of the second-order SM model, as discussed in [32, 33]. However, some modifications of Eq. (1) [34, 35] for active power (P), reactive power (Q), electromotive force (e) and electrical torque (T_e) are required as basic considerations for the proposed model:

$$\begin{cases} P = \omega M_f i_f \langle i, \sin\theta \rangle \\ Q = -\omega M_f i_f \langle i, \cos\theta \rangle \\ T_e = M_f i_f \langle i, \sin\theta \rangle \\ e = \omega M_f i_f \langle i, \sin\theta \rangle - M_f \dfrac{di_f}{dt} \langle i, \cos\theta \rangle \\ \qquad\quad = \omega M_f i_f \sin\theta \end{cases} \tag{1}$$

where ω is virtual angular frequency, i is grid current, θ is virtual rotor angle, $\langle .,. \rangle$ represents the conventional dot product for a three-phase system (as discussed in [33]), and $M_f i_f$ is field excitation. The $M_f i_f$ in this case would be modified in such a way that the output voltage of the FCS rectifier would adequately match the charging voltage of the EV battery regardless of changes in the FCS load. The active power-frequency loop, as shown in Fig. 1, was modified to aid the proposed controller's fast and dynamic tracking response to power and frequency changes, which will be discussed in the next subsection.

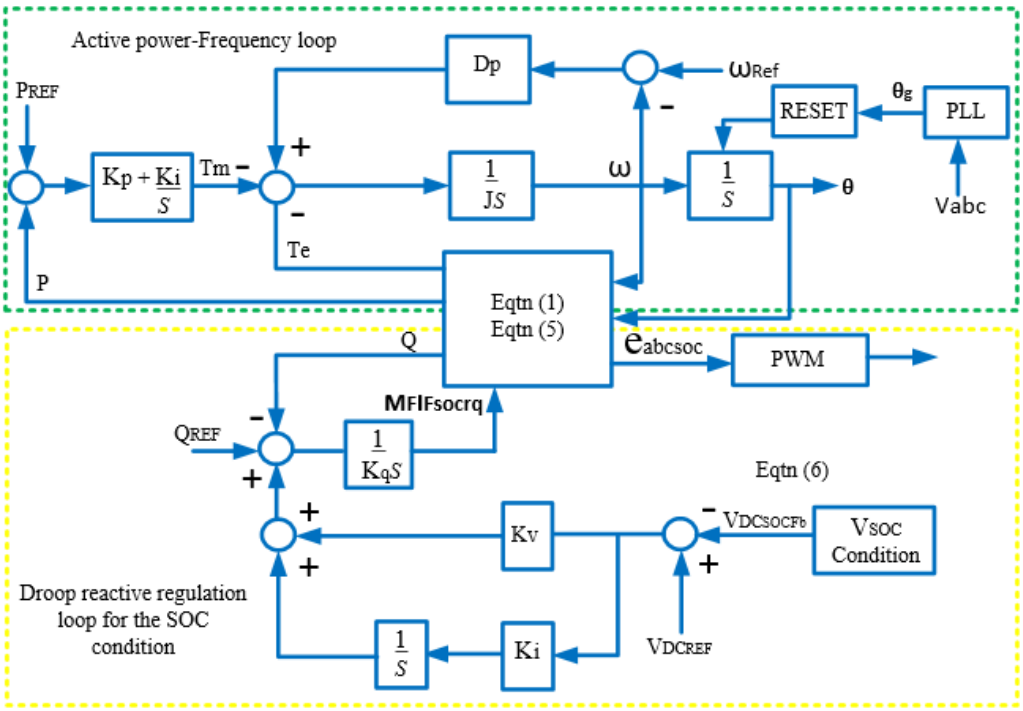

Fig. 1. Proposed controller with SOC feedback controller.

2.1. Proposed Active Power-Frequency Loop

As can be seen from the active power-frequency loop in Fig. 1, the mechanical torque (T_m) generated is obtained from the tracking error between reference active power (P_{Ref}) and active power (P). This tracking error value is fed to a PI controller, and the modified signal is passed through an integrator. The frequency droop aspect ensures frequency regulation by comparing the virtual angular frequency (ω) with the reference angular frequency (ω_{Ref}), and the difference is multiplied by the frequency loop feedback gain constant (D_p) and then added to the active torque (T_m). The regulation of P is achieved from the nested structure in the active power-frequency loop section, which comprises the inner loop of D_P and P with the feedback from the electric torque (T_e). The value of D_p can be obtained by dividing the inertia (J) by the time constant of the frequency feedback gain ($D_p=J/\tau_k$). For this concept to work effectively, the rectifier's frequency should be close to or the same as the grid angle (θ_g) to reduce the settling time when the FCS rectifier is connected to the power supply. This can be achieved through a phase-lock loop (PLL) to reset the integrator and θ_g, as shown in the highlighted active power-frequency loop. In this study, the improvement to the VSM model was the addition of the SOC configuration, which is explained in detail next.

2.2. Proposed Droop Reactive Regulation for SOC Condition as New Parameter İnput to VSM

The droop strategy for the decoupling of active power-frequency (P-F) and reactive power-voltage (Q-U) loops, which was formulated based on [31,35], provided the fundamentals for the improvement of the VSM. As it was based on the droop technique, the hypotheses for the proposed controller were:

- The controller's inertia will be adapted in accordance with the EV battery's initial SOC to regulate the reactive power balance loop to withstand any transient changes in grid power exchange and for voltage and frequency stability at the PCC when multiple EVs are being charged at the same time.
- The SOC feedback voltage will ensure real-time adjustment of the charging voltage and current to match the SOC condition of the EV battery through the reactive power regulation loop and resist any rapid changes in power exchange to aid in an efficient and stable charging process.

Moreover, this study implemented reactive power regulation (Q_{rq}), which can be achieved during the charging mode to aid in the tracking of the reference reactive power (Q_{Ref}). In order to achieve the integration of the real-time adjustment of Q_{rq}, the value of Q_{Ref} can be set as 0 such that the tracking error between Q_{Ref} and Q is multiplied by a gain of $1/K_q$, where K_q is the VSM gain constant, and fed to the integrator to generate M_fi_f. By altering the setting of Q in Eq. (1), Q_{rq} for the SOC condition in real time can be derived, as shown in Eq. (2):

$$Q_{rq} = \frac{1}{Kq}(Q_{Ref} - Q) \tag{2}$$

Where K_q is the VSM gain constant for the reactive power regulation due to the active power exchange under the SOC condition ($1/K_q=K_q$, if the steady-state error is neglected), and this forms the first part of the proposed controller's

droop reactive regulation under the SOC condition. In the second part, the FCS rectifier's automatic voltage regulation under the SOC condition (V_{SOCrq}) generates the required excitation (M_fI_{fsocrq}).

In order to generate M_fI_{fsocrq} in the proposed droop reactive regulation loop under the SOC condition, as shown in Fig. 1, the V_{SOCrq} loop is added to the Q_{rq} loop. Firstly, V_{SOCrq} is established by considering the droop relationship illustrated in Fig. 2. Power is transferred to the EV battery when the active power flow to the battery is needed. This droop concept is used when there is a sudden change in the power flow from the rectifier due to the SOC (V_{DCSOC}) condition to the EV battery due to the load change at the PCC. Through this approach, the VSM would be able to adapt a constant charging voltage under the SOC condition, while maintaining reactive power injection to the grid.

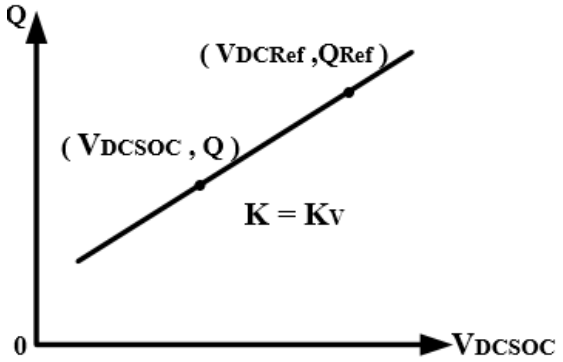

Fig. 2. Droop curve based on EV battery's SOC condition.

Therefore, the FCS rectifier's voltage (V_{DCSOC}) and the reactive power's (Q) adaptability to the SOC condition (Q-V_{DCSOC}) with respect to V_{SOCrq} can be represented as in Eq. (3):

$$\begin{cases} Q = Q_{Ref} - K_v(V_{DCRef} - V_{DCSOC})\ (K_v > 0) \\ \dfrac{Q}{Q_{Ref}} = V_{socrq} = K_v(V_{DCRef} - V_{DCSOC}) \end{cases} \quad (3)$$

Where V_{DCSOC} is the FCS rectifier's output voltage due to the SOC, V_{DCRef} is the reference FCS rectifier's output voltage and K_v is the voltage regulation constant due to the SOC. The value of K_v must be in the range from 0 to 1 for an effective automatic regulation of charging (Y) under the SOC condition and to prevent discharging (X) during the FCS operation. By neglecting losses due to active power exchange, the value of K_v can also be D_q ($K_v = D_q$). Similarly, an adjustment can be made and Eq. (3) is rewritten such that V_{DCSOC} =Vsoc=$V_{DCSOCfb}$ for an instantaneous V_{SOCrq} during charging, as shown in Eq. (4):

$$\begin{cases} V_{socrq} = \begin{cases} 0 \le SOC \le X \\ X \le SOC \le Y = K_v(V_{DCRef} - V_{DCSOCfb}) \\ Y < SOC \le 1 \end{cases} \\ K_v = \dfrac{Q_{Ref} - Q}{(V_{DCRef} - V_{DCSOCfb})} = \dfrac{K_q}{\tau_k Q_{Ref}} \end{cases} \quad (4)$$

where $V_{DCSOCfb}$ is the feedback voltage generated instantaneously from the rectifier's output and τ_k is the time constant for the droop loop (J/D_p).

Therefore, as shown in Fig. 1 of the proposed droop reactive regulation loop with the SOC condition as the new parameter input for the VSM, the difference between V_{DCRef} and $V_{DCSOCfb}$ is the tracking error that needs to be controlled. This tracking error is multiplied with K_v to give the output signal to be added, with the tracking error feedback signal also multiplied with an integral constant (K_i), and both are passed through the integrator. The error signal generated is added to the tracking error between Q_{Ref} and Q, which is obtained according to Eq. (2). The output of the resulting signal is fed to an integrator of gain $1/K_q$ to generate M_fI_{fsocrq} , where M_fI_{fsocrq} functions as the field excitation due to the SOC condition and adapts the virtual inertial to ensure the adjustment to the SOC condition in the FCS controller. Thus, combining Eqs. (2) and (4) gives the expression for M_fI_{fsocrq}. Substituting M_fi_f = M_fI_{fsocrq} into Eq. (2), the electromotive force due to the SOC consideration (e_{abcsoc}) of the FCS controller can also be estimated as in Eq. (5):

$$\begin{cases} M_fI_{f_{socrq}} = Q_{rq} + V_{socrq} \\ \qquad = \dfrac{1}{Kq}(Q_{Ref} - Q) + K_v(V_{DCRef} - V_{DCSOCfb}) \\ e_{abcSOC} = \omega M_fI_{f_{socrq}} \sin\theta \end{cases} \quad (5)$$

Relatedly, the e_{abcsoc} signal is fed to the pulse-width modulation (PWM) for pulse generation. The proposed VSM link to the SOC condition can be generally presented as in Eq. (6):

$$VSM_{M_fI_{fsocrq}} = \frac{1}{Kq}(Q_{Ref} - Q) + K_V(V_{DCRef} - V_{DCSOCfb}) \quad (6)$$

The i-VSM-based FCS using the single-stage three-phase PWM rectifier with the SOC feedback controller was simulated, and the results and analysis are presented in the next section.

3. Result and Simulation Analysis

In order to examine the robustness and effectiveness of the proposed strategy. The control technique proposed in this paper is achieved via the VSM droop control algorithm through the feedback voltage from the FCS output ($V_{DCSOCfb}$), integrated into in the reactive power loop. The $V_{DCSOCfb}$ at SOC condition is used to control the reactive power injection to the grid at SOC consition of the EV battery. This concept ensures the adjustment of the of the output power based on the grid's voltage or frequency deviation to optimize the EV battery charging process at SOC condition. Such that, when the grid voltage or frequency varies from the nominal values due to changes in the load profile of the FCS, the VSM's output power and inertia is adapted in proportion to these variations to ensure a stable charging process and provide grid stability. The test simulation system with the proposed VSM control presented in Fig. 1 was developed and built in MATLAB/Simulink, as shown in Fig. 3.

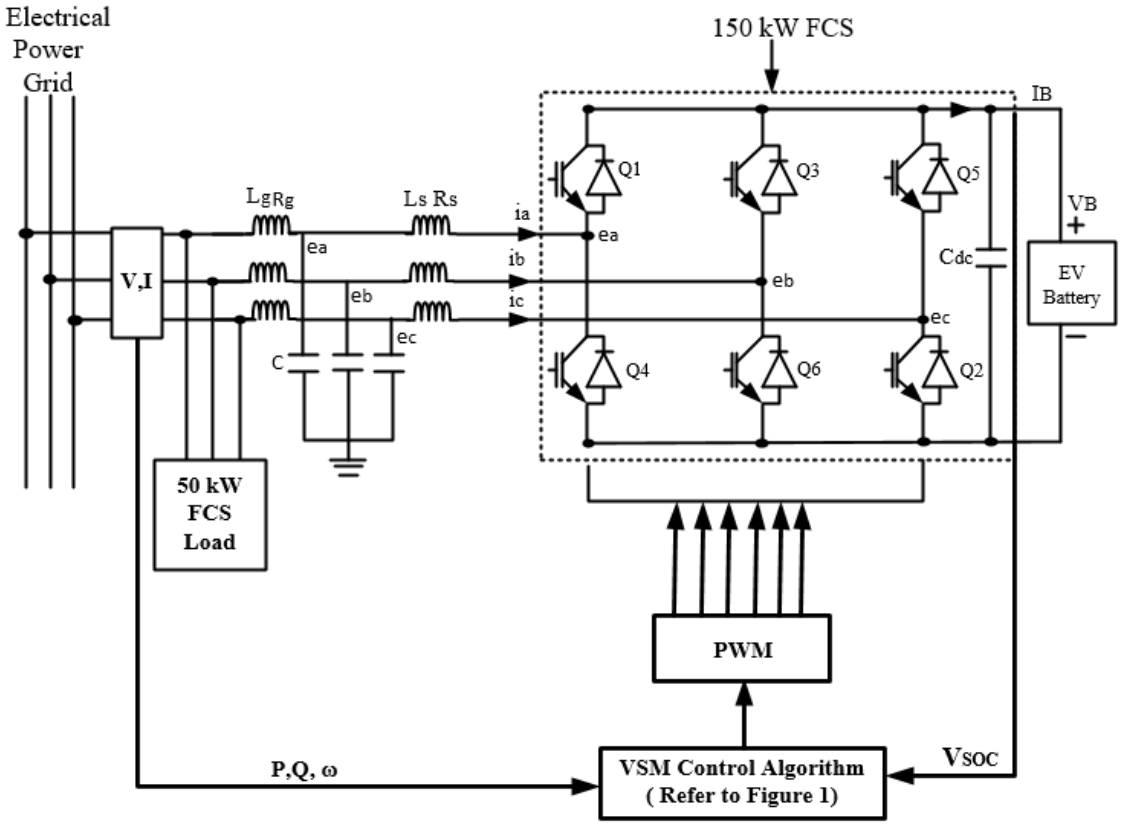

Fig. 3. Proposed i-VSM-based FCS using single-stage three-phase PWM rectifier at PCC**.**

The solver and the relative tolerance for the simulations are given as ode23t and 10^{-3} with a maximum step size of 10 μs, respectively. The simulation parameters for the proposed model are presented in Table 1. The source of simulation parameters in Table 1, are modified from two stage converter topology in [22, 33], through try and error method to demonstrate the possibility of this novel charging of the 100 Ah lithium battery with associated parameter in Simulink model.

Table 1. Simulation parameters of proposed model

Types	Parameter	Value
Filter parameters	Filter inductor (L)	1500 μH
	Filter capacitor (C)	15 μF
FCS system parameters	AC voltage of grid (V_{abc})	380 V
	Switching frequency for rectifier	10 kHz
	DC link capacitor (C_{DC})	1500 μF
	FCS reference output voltage	470 V_{DC}
	Nominal voltage	400 V
EV battery parameters	Rated frequency (θ_g)	50 Hz
	Battery rated capacity	100 Ah
VSM control parameters	VSM inertia coefficient (J)	0.1 kgm^2
	Pole pairs	1
	Voltage regulation constant (K_v)	0.5
	VSM gain constant (K_q)	114
	Reference value of active power (P_{Ref})	150 kW
	Reference value of reactive power (Q_{Ref})	0 Var
	VSM integral constant (K_i)	0.4

	VSM stator inductance (L_S)	0.0049 H
	VSM stator resistance (R_S)	0.1 Ω

3.1. Verification of Proposed FCS Controller's Performance on EV battery

A lithium-ion battery model was adopted in Simulink to test the proposed controller's behavior and adaptability to the SOC condition. The proposed i-VSM-based FCS was connected to the grid for 20 s of simulation time. The initial SOC and the EV battery response time were set at 50% and 1 s, respectively, for the simulation. Fig. 4 shows a consistent rise to 51.79% of the SOC at 20 s, while Fig. 5 and Fig. 6 show a corresponding adaptable charging voltage of 461.4 V_{DC} and a steady charging current of 325 A supplied to the EV battery respectively.

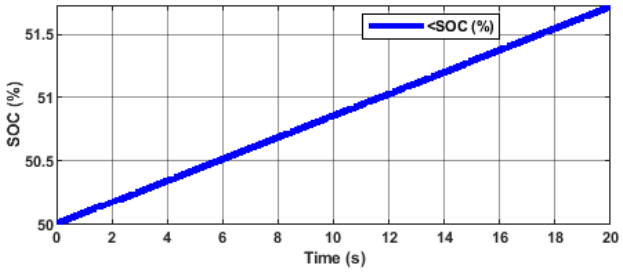

Fig. 4. Verification of proposed FCS controller's SOC performance with respect to time for EV battery capacity during charging.

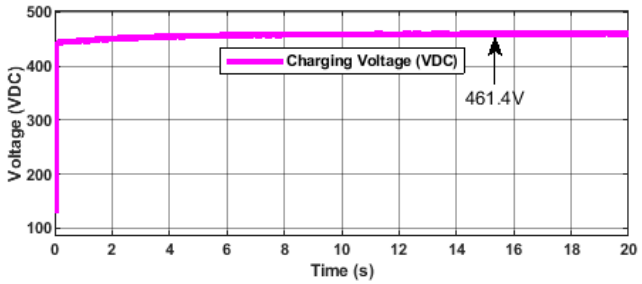

Fig. 5. Verification of proposed FCS controller's charging voltage performance with respect to time for EV battery capacity during charging.

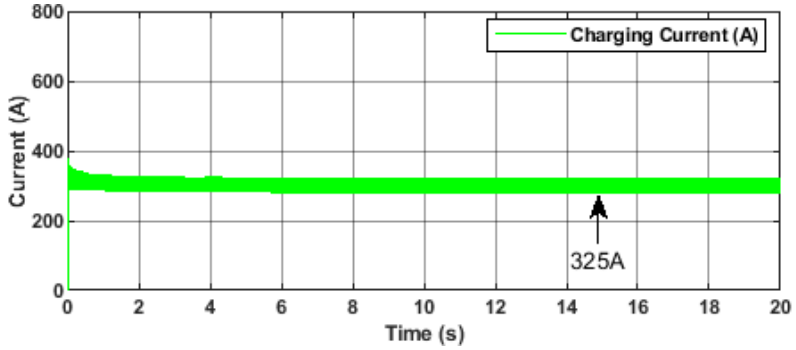

Fig. 6. Verification of proposed FCS controller's charging current performance with respect to time for EV battery capacity during charging.

Figure 7 shows that during the charging process, the proposed controller was able to maintain a nominal discharge current of 43.4783 A and discharge rate (C-rate) of 0.4347 C (details of the C-rate's allowable margin can be found in [36]). The nominal current discharge characteristic curve was used as a reference point to ascertain the effectiveness of the proposed controller in enabling an optimal charging performance to aid in prolonging the life span of the battery during the discharging motor mode. Different initial SOC values were applied to ensure that the charging voltage was adjusted based on the EV battery's SOC condition by the controller at transient in a manner similar to that of the SM.

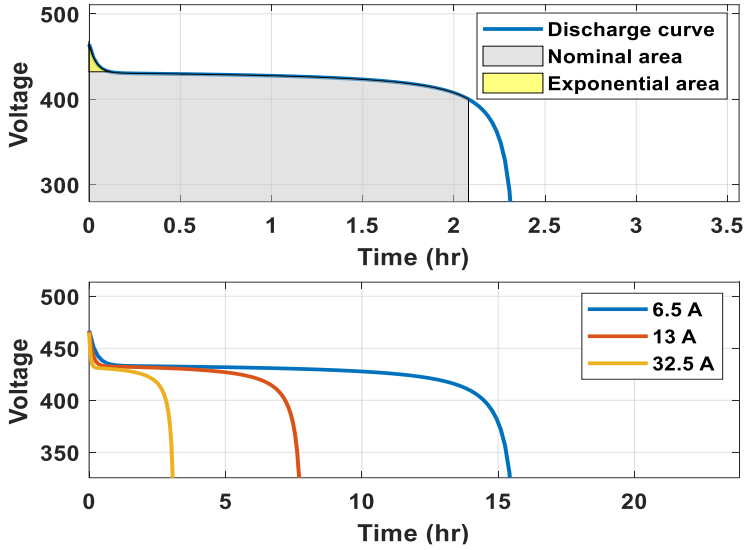

Fig. 7. Nominal current discharge characteristics of 100Ah EV battery (at 0.43478C, 43.4783A).

To further verify the effectiveness and adaptability of the proposed controller to different SOC conditions, the simulation time was set to 20 s and the battery response time was maintained at 1s. Simulations were carried out for different initial SOC values (50%–80%) for the 100Ah EV battery and the results are presented in Table 2.

Table 2. Simulation results at different initial SOC values (50%–80%)

S/N	Initial SOC value (%)	CC (A)	CV (V_{DC})	PF	SOC at 5 s (%)
1	50	325.0	461.4	0.9150	50.79
2	60	322.4	465.1	0.9158	60.79
3	70	320.7	467.4	0.9317	70.79
4	80	319.2	469.8	0.9429	80.79

Notes: CC: Charging current, CV: Charging voltage, PF: Power factor (PF=Real Power (P)/Apparent Power($\sqrt{(P2+Q2)}$) = Watts/Volt-Amps)

Table 2 shows that the proposed controller gave the necessary amount of charging current and maintained the charging voltage to the EV battery based on the initial SOC value to prevent overcharging. The impact of this concept on power factor and grid frequency at the PCC was verified to be in conformity with IEEE Std. 1547 [37] for all SOC conditions simulated for the 100Ah lithium EV battery at different SOC initial values of 50%–80%.

3.2. Verification of Proposed i-VSM Controller's Stability at PCC

The simulation time was set to 20 s with initial SOC of 50% and EV battery response time of 1 s. Fig. 8 shows that the proposed controller was able to give a constant active power exchange between the FCS and the electrical grid with minimum overshoots and was able to follow the reference power target. Fig. 9 shows that reactive power of 0 Var was injected into the grid in order to have a unidirectional flow to the EV battery under the SOC condition. Fig. 10 shows that the proposed controller's inertia ensured that grid frequency was maintained at the nominal set value during the FCS operation.

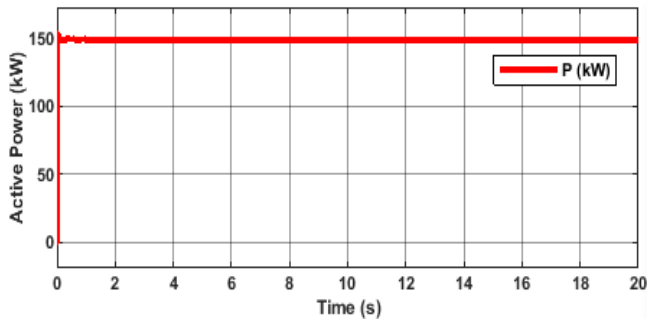

Fig. 8. Proposed controller's active power exchange stability at PCC with respect to time.

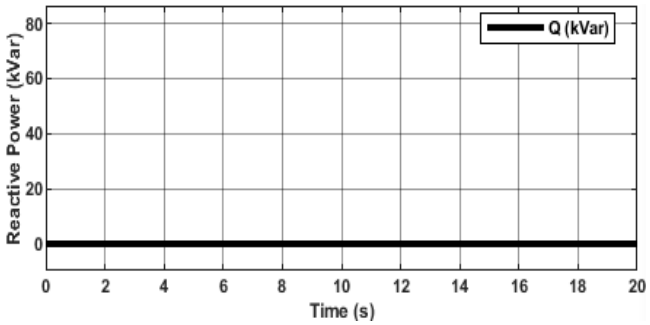

Fig. 9. Proposed controller's reactive power flow stability at PCC with respect to time.

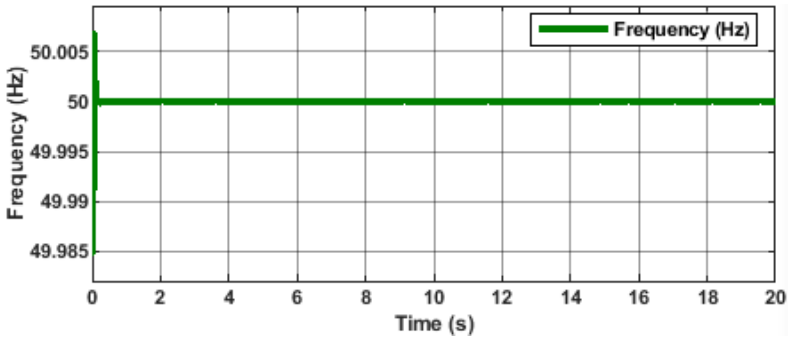

Fig. 10. Proposed controller's frequency adaptability at PCC with respect to time.

Furthermore, the interaction of the proposed model with other load at PCC in terms of power exchange stability was tested with different loads. Fig. 11 shows that when a 50kW load was applied at 0.5 s, the power exchange increased from 0 kW to 50 kW; additionally, when the proposed controller-based FCS of 150 kW load was applied at 2 s, the power exchange increased from 50 kW to 200 kW (50 kW +150 kW). The proposed controller was shown to provide an adjustment of the feedback mechanism to balance and adapt to the change in the active power exchange at the grid (50 kW + 150 kW) with negligible oscillation. Fig. 12 shows that the proposed controller's inertia adapted to the load changes and maintained grid frequency to the nominal set value.

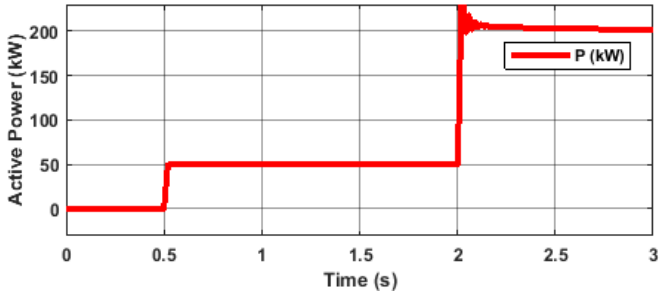

Fig. 11. Proposed controller's active power exchange stability impact at PCC due to sudden load changes with respect to time.

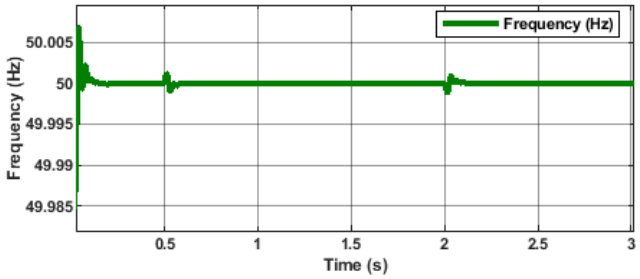

Fig. 12. Proposed controller's frequency adaptability stability impact at PCC due to load changes to time.

Consequently, Fig. 13 shows that the three-phase grid voltage waveforms at the PCC were in conformity with IEEE Std. 1159 [38]. The grid current waveforms and the phase voltage and current of the grid are presented in Fig. 14 and Fig. 15, respectively as below.

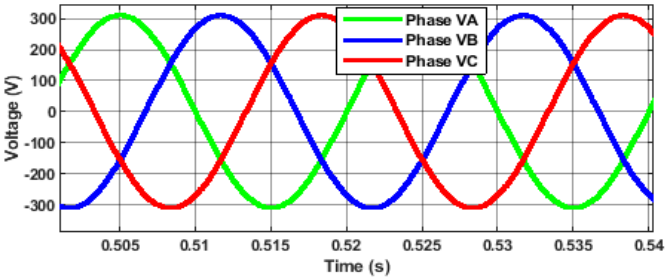

Fig. 13. Simulation results of the grid-side voltage waveform.

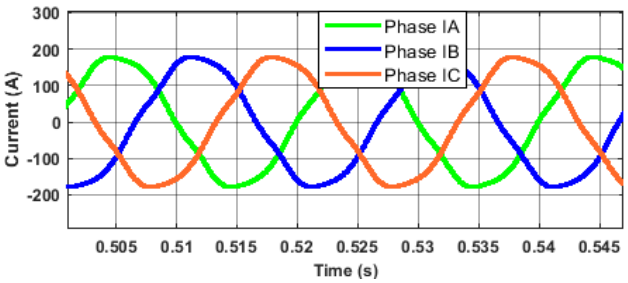

Fig. 14. Simulation results of the grid-side current waveform.

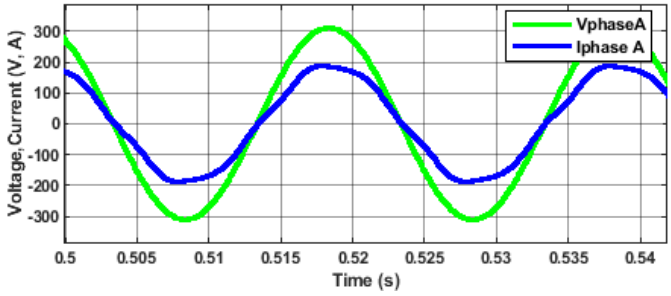

Fig. 15. Simulation results of the grid-side phase voltage and current.

3.3. Verification of Grid-Side Total Harmonic Distortion (THD) at PPC

Fig.16 shows the grid current output obtained for the FCS under the influence of the proposed controller in the fast Fourier transform (FFT) window at 2 dimensions of 5 cycle of the selected grid current signal. Fig. 17 shows that the grid-side current THD was at 3.67% for the FCS rectifier when the proposed i-VSM model combined with the SOC voltage feedback controller was used. This provided minimal current total harmonic distortion (THDi), which complied with IEEE Std. 519.

The novelty of this paper demonstrates an innovative concept of using $V_{DCSOCfb}$ as the new input parameter to the VSM, to ensure that the FCS can adjust voltage levels based on SOC condition to prevent overcharging. By adapting the charging voltage and current level as shown in Table 2, according to the EV battery's initial SOC, the FCS can maximize the C-rate as shown in Fig. 7, to aid efficiency of the charging process. This novelty allows the VSM to adapt the inertia to aid frequency regulation, stability of the active and reactive power exchange decoupling at any SOC condition, and to reduce oscillation and grid stress during peak demand periods as demonstrated in Figs. 8 and 9 at PCC with other connected nonlinear load for future multiple FCS application.

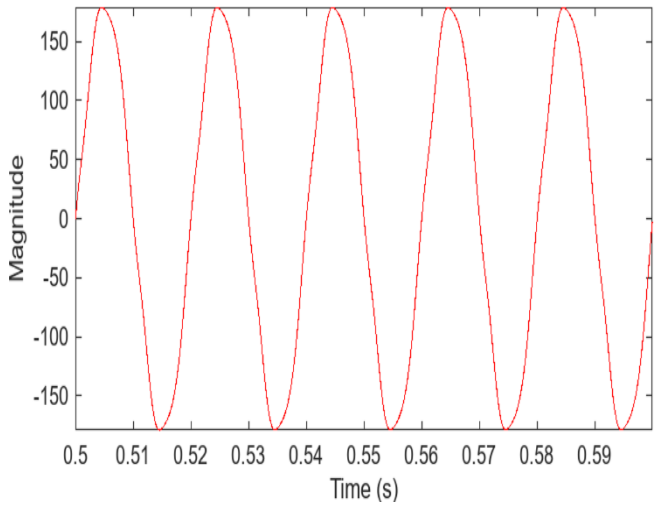

Fig. 16. FFT waveform of grid-side current of FCS rectifier with the proposed controller.

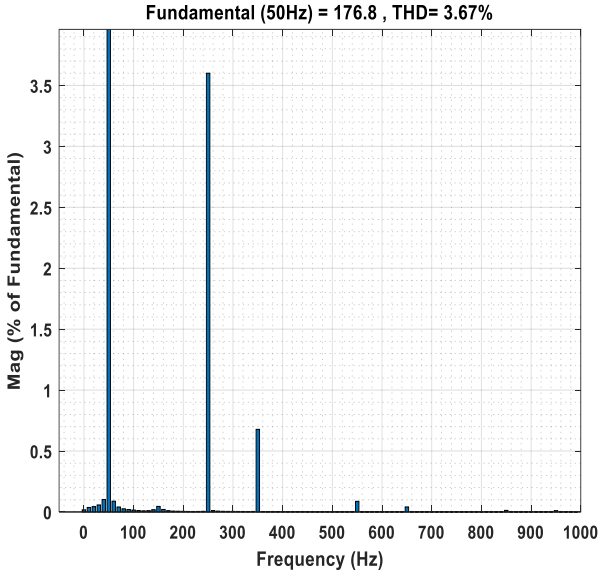

Fig. 17. FFT analysis of grid-side current harmonics of FCS rectifier with the proposed controller.

4. Conclusion

The SOC voltage feedback controller for an i-VSM-based FCS is proposed in this paper. In this control, virtual inertia ensured real-time adaptability to any changes in the EV battery's SOC condition to aid in the controller's transient and dynamic responses during the FCS operation. The proposed controller was modeled and verified using simulations with parameters presented in Table 1 to prove its adaptability to the EV battery's SOC and its ability to stabilize grid voltage, frequency and reactive power decoupling regulation at above 0.9 power factor. The relationships established in Figs. 4–17 show that the proposed controller used the initial SOC value to regulate the real-time charging process of the EV battery.

Furthermore, the SOC feedback mechanism helped to continuously adapt and adjust to the EV battery's initial SOC parameter to enhance the charging process. The proposed controller responded to the changes in the power flow from the AC source and, with a constant FCS load profile, it gave close to unitary power factor at the PCC. In addition, the proposed controller maintained the power exchange at the PCC with minimal oscillation regardless of load changes. The proposed control strategy ensured a minimized impact on the power grid by providing virtual inertia support to aid in charging the EV battery in a very short time, while preventing overcharging and hence maintaining the life cycle of the EV battery. The proposed strategy effectively simulated the advantages of the droop concept in SMs. Since Q is proportional voltage balanced at the grid, by adjusting the field excitation in the reactive power loop in accordance with the functioning condition of the EV battery's SOC feedback voltage, the proposed controller gave a swift dynamic response unlike those of other VSM-based PI controllers, as hypothesized in this paper. Consequently, the following deserving future directions of this novel concept were proposed by the paper's authors for further development:

- Stability analysis for the novel single stage VSM based FCS with SOC feedback controller for E-mobility grid

infrastructure inertia reinforcement for multiple EV battery charging condition.

- A neural-network based comparison of the developed VSM with SOC feedback controller for EV battery state of health detection and inertia adaptability during multiple EV battery charging process.

Acknowledgements

This research was supported by Universiti Tun Hussein Onn Malaysia (UTHM) through Tier 1 (vot Q365), Centre for graduate studies (CGS-UTHM), the Zurich University of Applied Sciences and the Advanced Control in Power Converter research group in FKEE, UTHM for financial and technical assistance. At the same time to the Ministry of Higher Education (MOHE) of Malaysia for the scholarship assistance from the Malaysian International Scholarship initiative.

References

[1] S. A. Zulkifli, and K. Momoh, "Grid stability ımprovement for charging stations of EV battery during V2G", IEEE Smart Grid Bull. Compend. USA,vol. 27, pp.18-19, November 2022.

[2] J. Chen, and H. Chen, "Research on the planning of electric vehicle fast charging stations considering user selection preferences", Energies, Switzerland, vol. 16, pp.1-22, February 2023.

[3] E. Garba, S.A. Zulkifli, S. Z. Iliya, H. Bevrani, K. Momoh, M. H. Khan, and M. Ahmed "Deadbeat current control in grid-connected ınverters: a comprehensive discussion", IEEE Access, USA, vol. 10, pp. 3990-4014, December 2021.

[4] M. M. Mahfouz, and R. Iravani, "Autonomous operation of the DC fast-charging station", IEEE Trans. Ind. Electron. USA, vol. 69, pp. 3787-3797, April 2022.

[5] H. S. Salama, S. M. Said, I. Vokony, and B. Hartmann, "Adaptive coordination strategy based on fuzzy control for electric vehicles and superconducting magnetic energy storage - towards reliably operating utility grids", IEEE Access,USA, vol. 9, pp. 61662-61670, April 2021.

[6] Y. Sehimi, J. Sakly, K. Almaksour, and B. Robyns, "A novel fast charger architecture with reduced ımpact on distribution grids based on V2V power transfer", 2021 IEEE Veh. Power Propulsion Conference, Spain, pp.1-6, 25-14 November 2021.

[7] V. Mallemaci, F. Mandrile, S. Rubino, A. Mazza, E. Carpaneto, and R. Bojoi, "A comprehensive comparison of virtual synchronous generators with focus on virtual inertia and frequency regulation", Electr. Power Syst. Res. Switzerland, vol. 201, pp.107516-107529, August 2021.

[8] K. Momoh, S. A. Zulkifli, P. Korba, F. R. S. Sevilla, A. N. Afandi, and A. Velazquez-Ibañez, "State-of-the-art grid stability ımprovement techniques for electric vehicle fast-charging stations for future outlooks", Energies, Switzerland, vol. 16, pp.1-29, May 2023.

[9] L. Camurca, T. Pereira, F. Hoffmann, and M. Liserre, "Analysis, limitations, and opportunities of modular multilevel converter-based architectures in fast charging station infrastructure", IEEE Trans. Power Electron.USA, vol. 37, pp.10747-10760, September 2022.

[10] R. Jackson, S. A. Zulkifli, N. M. B. Sham, and E. Pathan, "A self-frequency restoration control based on droop strategy for autonomous microgrid", Int. J. Renew. Energy Res. Turkey, vol. 9, pp. 749-756, June 2019.

[11] N. M. Ahmed, M. Ebeed, K. Sayed, A. Alhejji, and A. Refai, "Robust cascaded controller for load frequency control in renewable energy ıntegrated microgrid containing PEV", Int. J. Renew. Energy Res. Turkey, vol. 13, pp. 435-445, March 2023.

[12] A. Kilic, "Analysis of charging systems for electric vehicle", Int. J. Smart Grid, USA, vol. 7, pp. 177-186, September 2023.

[13] A. Gamawanto, M. U. Qinthara, F. S. Rahman, K. M. Banjar-Nahor, and N. Hariyanto, "Pricing scheme for ev charging load penetration in distribution network: study case Jakarta", 7th International Conference on Smart Grid (icSmartGrid 2019), Australia, pp. 159-164, 9-11 December 2019.

[14] G.Ala, A.O. Di Tommaso, R. Miceli, C. Nevoloso, G. Scaglione, G. Schettino, and F. Viola, "Virtual synchronous generator: an application to microgrid stability", 11th IEEE International Conference on Renewable Energy Research and Applications (ICRERA 2022), Istanbul, pp. 151-157,18-21 September 2022.

[15] A. Gezer, B. Z. Unver, and E. Bostanci, "Optimal battery sizing for electric vehicles considering battery ageing", 11th IEEE International Conference on Renewable Energy Research and Applications (ICRERA 2022), Istanbul, pp. 82-89, 18-21 September 2022.

[16] M. Maaruf, S. El Ferik, F. Saleh Al-Ismail, and M. Khalid, "Robust optimal virtual ınertia control for microgrid frequency regulation considering high renewable energy penetration", 11th IEEE International Conference on Renewable Energy Research and Applications (ICRERA 2022), Istanbul, pp. 369-373, 18-21 September 2022.

[17] W. Sang, W. Guo, S. Dai, C. Tian, S. Yu, and Y. Teng, "Virtual synchronous generator, a comprehensive overview", Energies, Switzerland, vol. 15, pp. 1-29, September 2022.

[18] Y. Tao, J. Qiu, S. Lai, X. Sun, and J. Zhao, "Adaptive ıntegrated planning of electricity networks and fast charging stations under electric vehicle diffusion", IEEE Trans. Power Syst. USA, vol. 38, pp. 499–513, January 2023.

[19] F. Mandrile, D. Cittanti, V. Mallemaci, and R. Bojoi, "Electric vehicle ultra-fast battery chargers: A boost for power system stability?", World Electr. Veh. J. Switzerland, vol. 12, no. 1, pp. 1-21, January 2021.

[20] Z. Yang, C. Mei, S. Cheng, and M. Zhan, "Comparison of ımpedance model and amplitude-phase model for power-electronics-based power system", IEEE J. Emerg. Sel. Top. Power Electron. USA, vol. 8, pp. 2546-2558, September 2020.

[21] N. A. Mohd Yusoff, A. M. Razali, K. Abdul Karim, A. Jidin, and T. Sutikno, "An analysis of virtual flux direct power control of three-phase AC-DC converter", Int. J. Power Electron. Drive Syst. Indonesia, vol. 9, pp. 947-956, September 2018.

[22] X. Yan, F. Qin, J. Jia, Z. Zhang, X. Li, and Y. Sun, "Virtual synchronous motor based-control of Vienna rectifier", 7th International Power and Energy Systems Engineering Conference (CPESE 2020), Japan, pp. 953-963, 26-29 September 2020.

[23] Q. Zhang, D. Gan, Z. Zhang, J. Li, and Y. Luo, "A method for evaluating the ımpact of controllers and wind turbine generators on low-frequency oscillation", IEEE Access, USA, vol. 11, pp. 37461–37471, April 2023.

[24] J. L. Rodriguez-Amenedo, S. A. Gomez, M. Zubiaga, P. Izurza-Moreno, J. Arza, and J. D. Fernandez, "Grid-Forming control of voltage source converters based on the virtual-flux orientation", IEEE Access,USA, vol. 11, no.1, pp. 10254–10274, January 2023.

[25] I. Aretxabaleta, I. M. D. E. Alegría, and J. O. N. Andreu, "High-Voltage stations for electric vehicle fast-charging: trends, standards, charging modes and comparison of unity power-factor rectifiers", IEEE Access,USA, vol.9, pp.102177–102194, June 2021.

[26] K. M. Cheema, N.I. Chaudhary, M. F. Tahir, K. Mehmood, M. Mudassir, M. Kamran, A.H. Milyani, and Z.M. Salem Elbarbary "Virtual synchronous generator: Modifications, stability assessment and future applications", Energy Reports, United Kingdom, vol. 8, pp. 1704–1717, December 2022.

[27] K. Bi, Y. Xu, P. Zeng, W. Chen, and X. Li, "Virtual flux voltage-oriented vector control method of wide frequency active rectifiers based on dual low-pass filter", World Electr. Veh. J. Switzerland, vol. 13, pp. 1–13, February 2022.

[28] L. Yan, Z. Zhu, J. Qi, Y. Ren, C. Gan, S. Brockway, and C. Hilton "Enhancement of disturbance rejection capability in dual three-phase PMSM system by using virtual ımpedance", IEEE Trans. Ind. Appl.USA, vol. 57, pp. 4901–4912, October 2021.

[29] Q. Lin, H. Uno, K. Ogawa, Y. Kanekiyo, T. Shijo, J. Arai, T. Matsuda, D. Yamashita, and K. Otani "Field demonstration of parallel operation of virtual synchronous controlled grid-forming ınverters and a diesel synchronous generator in a microgrid", IEEE Access,USA, vol. 10, pp. 39095-39107, April 2022.

[30] J. Gupta, and B. Singh, "Based high power factor single stage charging solution for light electric vehicles", IEEE Trans. Ind. Appl. USA, vol. 58, pp. 732-741, February 2022.

[31] X. Yan, J. Li, B. Zhang, Z. Jia, Y. Tian, H. Zeng, and Z. Lv, "Virtual synchronous motor based-control of a three-phase electric vehicle off-board charger for providing fast-charging service", MDPI Appl. Sci. Switzerland, vol. 8, pp. 1-14, May 2018.

[32] L. Chen, J. Tang, X. Qiao, H. Chen, and Z. Zhao, "Study of resistive SFCLs for transient stability enhancement of paralleled synchronous and virtual synchronous generators in weak grid", IEEE Trans. Ind. Appl.USA, vol. 59, pp. 3044-3055, June 2023.

[33] Z. Ma, Q. C. Zhong, and J. D. Yan, "Synchronverter-based control strategies for three-phase PWM rectifiers", 7th IEEE Industrial Electronics Applications Conference (ICIEA 2012), Singapore, pp. 225-230, 18-20 July 2012.

[34] F. An, J. Jiang, W. Zhang, C. Zhang, and X. Fan, "State of energy estimation for lithium-ıon battery pack via prediction in electric vehicle applications", IEEE Trans. Veh. Technol.USA, vol. 71, pp. 184–195, January 2022.

[35] Y. Tao, and W. Tang, "Virtual flux and positive-sequence power-based control of grid-interfaced converters against unbalanced and distorted grid conditions", J. Electr. Eng. Technol. South Korea, vol. 13, pp. 1265–1274, May 2018.

[36] H. Polat, F. Hosseinabadi, Md. Mahamudul Hasan, S. Chakraborty, T. Geury, M. El Baghdadi, S. Wilkins and O. Hegazy, "A review of DC fast chargers with bess for electric vehicles: topology, battery, reliability oriented control and cooling perspectives", Batteries, Switzerland, vol. 9, pp.1–36, February 2023.

[37] IEEE Standard 1547-2023, Recommended standard for interconnecting distributed resources with electric power system, The Institute of Electrical and Electronics Engineers, 2023.

[38] IEEE Standard 1159-2019, Recommended practices for monitoring electric power, The Institute of Electrical and Electronics Engineers, 2019.